



Pitting mechanism of mild steel in marginally sour environments – Part II: Pit initiation based on the oxidation of the chemisorbed iron sulfide layers

Wei Zhang*, Bruce Brown, David Young, Marc Singer

Institute for Corrosion and Multiphase Technology, Ohio University, 342 West State Street, Athens, OH, 45701, USA

ARTICLE INFO

Keywords:

- A. Mild steel
- B. Raman spectroscopy
- B. TEM
- C. Pitting corrosion
- C. Oxidation
- C. Pourbaix diagram

ABSTRACT

The role of trace concentrations of O₂ (ca. 20 ppb_(w)) relating to pitting in marginally sour environments was investigated in this work. Laboratory experiments were conducted with X65 mild steel specimens at pH 5.00 ± 0.01, 30 °C, 0.97 bar CO₂ and 0.04 mbar H₂S with/without O₂ for up to 7 days. Acquired corrosion rate, the composition of the corrosion product layer, and surface profile after the layer was removed were compared. As a result, only H₂S chemisorption layer was formed without oxygen; this layer could be partially compromised when [O₂]_{aq} > 3 ppb_(w), leading to pitting initiation.

1. Introduction

“Marginally sour” or “slightly sour” environment [1,2] features low temperature and a trace amount of H₂S. It has been reported that even a trace amount of H₂S in a CO₂ dominant environment (sweet) will decrease general corrosion rate by forming thin iron sulfide layers, but can increase the possibility of localized attack [1,3]. Previous studies [1, 3–7] have shown occurrences of localized corrosion, but have not fully revealed the mechanism of this type of pitting attack. The ratio of H₂S and CO₂ partial pressures [8] has been used to define this transition between sweet and marginally sour environments. However, this description has its limitations [9] as the occurrence of localized corrosion is related to the water chemistry and the state of the steel surface, not just the composition of the gas phase. Alternatively, the surface saturation degree of FeS and FeCO₃ at the steel substrate surface should be considered [1,2].

Localized corrosion is usually thought to initiate due to a localized failure of a protective layer formed on the steel surface. In general, the pit initiation mechanism remains fairly elusive, especially as it relates to how exactly the layer breaks down to induce pitting. For example, in O₂ containing systems, the effect of Cl⁻ is observed as an important detrimental factor in the breakdown of passive layers. According to Strehblow [10], there are three major interpretations of passive layer breakdown, all involving the effect of chloride ions: the penetration mechanism (diffusion of anion and cation vacancies through the passive layer), the film breaking mechanism (microcracks produced by potential

fluctuation), and the adsorption mechanism (the passive layer was dissolved by the complexation effect of aggressive ions such as SO₄²⁻). However, the characteristics of most sour corrosion product layers differ greatly compared to passive films and different breakdown mechanisms must be considered.

In CO₂ dominated environments, the corrosion product layer is often comprised of a mixture of FeCO₃, Fe₃C, and possibly iron oxides. FeCO₃ cannot be qualified as a passive layer as it is typically very thick (few microns). The formation of the layers in CO₂ corrosion could bring the open circuit potential higher ($\Delta E < 100$ mV) [11], but not as high as is typically the case in truly passive behavior. In addition, it has been hypothesized that the decrease in corrosion, accompanied by the formation of FeCO₃, is due mostly to the formation of a thin (few nm) iron oxide layer between the steel substrate and the FeCO₃ crystals [11]. This so called “pseudo-passive” layer, provides protection on uniform corrosion. Localized corrosion may initiate if the oxide layer coverage is not uniform. However, the relationship between potential and occurrence of pitting, typical of stainless steel for example, is not observed in CO₂ corrosion [11]. Therefore, there is no “critical potential” in CO₂ localized corrosion driving the initiation of localized corrosion. Mechanical damage of the layer could lead to pitting and has been attributed to the effect of fluid flow shear stress [12,13] and erosion [14]. However, it was found that except for cavitation, the shear force of the fluid flow is never high enough to damage an FeCO₃ layer [12]. Sun attributed the observation of damage to an FeS layer to internal stresses and the initiation to the microcracks within the corrosion product layer

* Corresponding author at: Schlumberger, Inc., 6350 W Sam Houston Pkwy N, Houston, TX 77041, USA.

E-mail addresses: wz521414@ohio.edu, giannazw@hotmail.com (W. Zhang).

[15]. However, the reported case cannot be applied in a wider scope because microcracks and defects are common in these precipitated layers, but pitting is not always there. Generally speaking, an incompletely generated layer, a partially dissolved layer, or a broken layer (by intrinsic stress or external mechanical forces) could be explanations for pit initiation. The characteristics of an incompletely generated layer or a partially dissolved layer is governed by local water chemistry. In CO₂ environments, the “grey zone” theory describes how such damages in the layer can develop and how localized corrosion can be initiated [16, 17]. The factors that can lead to localized corrosion of mild steel in H₂S/CO₂ environments are summarized in Fig. 1.

Part I paper of this research project [18] described the parametric study performed to identify the key parameters controlling the occurrence of pitting in marginally sour environments [2]. The baseline condition, for which severe pitting occurred, was selected at 30 °C, pH 5.00 ± 0.01, 0.97 bar CO₂, 0.04 mbar H₂S, 300 rpm stir bar, O_{2(aq)} ≈ 20–40 ppb_(w), 7 days. A very thin layer of FeS, thought to be mackinawite, formed within the porous iron carbide network of mild steel to retard general corrosion. Although the bulk aqueous environment was not saturated with respect to FeS, it was postulated that this layer formed by precipitation that occurred because of a higher saturation of iron sulfide within the porous iron carbide structure. This was due to water chemistry being inherently different close to an actively corroding surface. The surface characterization of the specimen surface after the experiment revealed that the corrosion product layer was a porous 100–300 nm layer of iron sulfides and iron oxides. SAED showed the phases in question to be mackinawite (FeS) and magnetite (Fe₃O₄). However, the existence of the oxide was not expected since O₂ content was thought to be very low [O_{2(aq)} ≈ 20 ppb_(w)].

Limited research has been reported on the effect of oxygen on CO₂ corrosion [19,20]. In the presence of CO₂ (pCO₂ > 0.5 bar) but without H₂S, ingress of oxygen below 100 ppb_(w) in the aqueous phase is commonly reported to have a negligible effect on general or localized corrosion. Noticeable effects are only observed with a dissolved O₂ content above 1 ppm_(w) [19,20]. More broadly, the formation of oxides in the absence of O₂ (or with only traces of O₂ present) has been observed by FIB-TEM underneath a FeCO₃ layer in a CO₂ environment. The formation of this oxide layer was accompanied by an increase in potential [11] and very high surface pH (pH 8) [21]. The pH near the steel surface was much higher than that in the bulk solution because the FeCO₃ corrosion product layers served as the mass transfer barrier. This oxide was proposed to be formed due to high pH value near the steel surface, not due to the dissolved O₂. This discontinuous character of the iron oxide layer was related to the initiation of localized corrosion in CO₂ environments.

In high-temperature H₂S environments, magnetite has been reported to be always found underneath iron sulfide [22]. It was proposed that this magnetite was formed by a precipitation reaction between water and steel at high temperature [reaction (1)], because the saturation degree of the Fe₃O₄ was much higher than for mackinawite at high temperature (~120 °C). The outer side of the Fe₃O₄ layer was also

reported to be converted partially into iron sulfide [23]. As partial pressure of H₂S increased, the outer layer was characterized as mackinawite, troilite, pyrrhotite, and pyrite [22]. The authors found that, at 25 °C, no magnetite was detected and mackinawite was the only product of corrosion [22]. However, there was one piece of information missing: the oxygen ingress content was not monitored during the experiments. This said, the experiments were performed in a closed autoclave, so O₂ ingress could be expected to be minimal.



In the simultaneous presence of O₂ (ppm level) and H₂S, several oxidized sulfur-containing compounds can form [24,25] that strongly influence uniform and localized corrosion. A number of research works deliberately blending a relatively large amount of oxygen (more than 500 ppm) into H₂S environments were performed to study the effect of oxygen on corrosion [24] and stress cracking [25]. Oxygen has been linked to the occurrence of localized corrosion and pH decreases in the aqueous solution in the high H₂S pressure environments [24]. In relation to the oil and gas production industry, Crolet [26] warned that oxygen is detrimental in sour corrosion environments because of acidification effects.

For low temperature low H₂S concentration experiments, if any oxide was found together with sulfide, usually it was considered as an aftereffect from specimen handling and analysis. Since CO₂ and H₂S gases continuously flow into the test cell, the concentration of dissolved oxygen in the aqueous solution is thought to be kept at a minimum. Mackinawite was found to be vulnerable to oxidation in the air, especially in the presence of water [27], heat [28], and light [29]. Therefore, the oxides found are often considered as the product of mackinawite oxidation during material analysis. In the glass cell experimental setup, the O₂ concentration in the liquid phase was measured at a level between 20–40 ppb_(w). The presence of low levels of oxygen in the system was mainly due to the test apparatus (small leakage around o-rings) and procedure (specimen insertion and retrieval), which led to limited ingress of air. As mentioned above, in the presence of CO₂ (pCO₂ > 0.5 bar) but without H₂S, noticeable effects of O₂ contamination are only visible with dissolved O₂ content above 1 ppm_(w) [19,20]. However, considering the high reactivity between H₂S and O₂, the presence of 20–40 ppb_(w) of O₂ in the aqueous phase may have a non-negligible effect, especially in marginally sour environments. In this work, a series of experiments was designed to investigate how O₂ content (<40 ppb_(w)) can affect the corrosion process, how oxides can form on the steel surface, and what roles these oxides may play in localized corrosion initiation.

2. Experimental setup and procedure

Two kinds of testing apparatuses were used in this study - they are shown in Fig. 2. Fig. 2(a) shows the original reactor “type (a)” with rubber stoppers in the lid for hanging steel specimens using nylon thread; this setup exhibited poor oxygen ingress control, with aqueous oxygen concentrations of around 20 ppb_(w). Fig. 2(b) presents the updated reactor “type (b)” featuring ports on the lid which enabled insertion and retrieval of specimens without risking O₂ contamination. This new design ensured that the concentration of O₂ in the aqueous phase could be maintained below 3 ppb_(w). Two different mixing elements were used: hanging specimens with stir bar agitated solution for the original reactor (type a), and fixed specimen holders with central rotating impeller for the updated glass cell setup (type b). While the impeller glass cell system provided better control over the chemistry and mass transfer characteristics, the two experimental setups yielded comparable results in term of corrosion. Both types of the cells were connected to a H-type ion exchange column to bring down the pH value in the solution to the set value during the experiments [30]. However, this system was only capable of correcting increases in pH (not

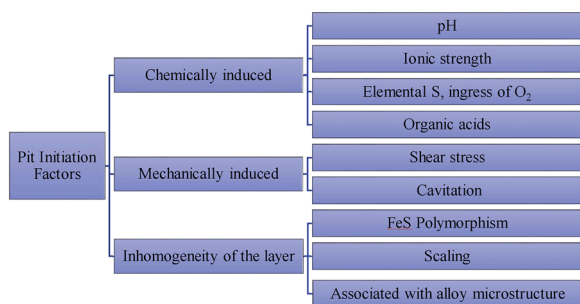


Fig. 1. Factors that can lead to localized corrosion of mild steel in H₂S/CO₂ environments.

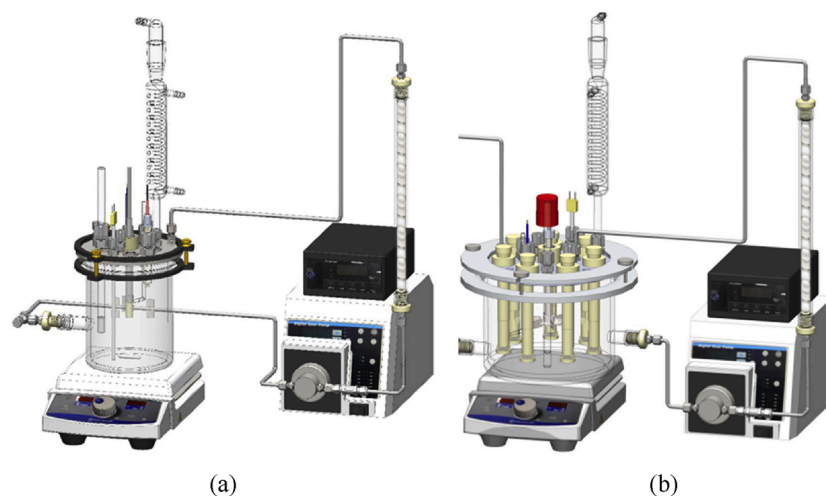


Fig. 2. Stable solution chemistry system for small scale lab test: (a) with hanging specimens and stir bar in a glass cell; (b) with fixed specimen holders and rotating impeller in a glass cell (images courtesy of Cody Shafer, ICMT).

decreases). The (a) type cell was used in the experiments with $[O_2]_{(aq)} \approx 20$ ppb_(w) or above, type (b) cell was used in the experiments with $[O_2]_{(aq)} < 3$ ppb_(w). Half square inch specimens made of API 5L X65 mild steel were used for corrosion testing in all the experiments. The chemical composition of the API 5L X65 steel is listed in Table 1 [31].

The experimental methodology is shown in Fig. 3. The procedure for both types of reactors is similar. First, the 1 wt.% NaCl electrolyte (pH was set to 5.01 ± 0.01) was sparged with CO₂ for over two hours, then with a mixture of H₂S and CO₂ for 30 min. This brought down the dissolved O₂ concentration in the system to the desired value. Four steel specimens were loaded to begin the corrosion experiment. Single specimens were retrieved after one day, three days and seven days of exposure for surface analysis by, on a select basis, scanning electron microscopy (SEM), energy dispersive X-ray spectroscopy (EDS), surface profilometry (for pitting measurement), Raman microscopy, and focused ion beam-transmission electron microscopy (FIB-TEM).

In order to investigate whether a trace amount of oxygen ingress would play a role in pitting in marginally sour environments, three experiments were conducted with an time average dissolved oxygen concentration below 3 ppb_(w), at 20 ppb_(w), and above 20 ppb_(w). As listed in Table 2, the other environmental conditions were identical: 30 °C, pH 5.01 ± 0.01 , 0.97 bar CO₂, 0.04 mbar H₂S, 300 rpm stir bar, 7 days. The other conditions were chosen based on the previous parametric study [2] where the most severe pitting happened.

3. Investigation of the origin of O₂ ingress and the formation of oxides

In order for any iron oxides to form in the sour corrosion test at low temperature and moderate pH, three scenarios were hypothesized:

- 1) The freshly polished steel surface could have been oxidized at the pre-processing stage, after the isopropanol and deionized water rinse but before loading into the glass cell.

- 2) The corrosion product layer, which formed during the experiment on the steel specimen, could have been oxidized after it was retrieved from the electrolyte and dried in the air before analysis.
- 3) Iron oxide could have formed in the liquid phase during the corrosion experiments.

A series of short experiments were designed to test each hypothesis. The corresponding method and results are listed together, considering each hypothesis, in Table 3.

It must be noted that iron oxidized could also be generated without the presence of oxygen; rather, it is a redirect reaction between iron and water. Based on the thermodynamics, iron could react with water directly at high temperatures or high pH [32]. As discussed in the introduction part, magnetite was found in high temperature and H₂S concentration environments, due to the higher saturation degree of Fe₃O₄ than any iron sulfides, as proposed by Gao et al. [22]. However, when it comes to the baseline condition at 30 °C and pH 5 in this work, this possibility of direct reaction is small. That is why this possibility was not proposed in Table 3.

To challenge the first hypothesis in Table 3, a Raman spectrum was collected from the freshly polished and isopropanol / deionized water rinsed X65 steel specimen (Fig. 4). The spectrum shows no oxides were present on the steel surface. This meant that no significant oxidation occurred before the steel specimen was loaded into the glass cell. Therefore, the first hypothesis was refuted.

To test the second hypothesis as shown in Table 3, a X65 specimen was immersed in a 1 wt.% NaCl electrolyte saturated with a gas phase of 0.97 bar CO₂ and 0.04 mbar H₂S at 30 °C, pH 5, and agitated with a 300 rpm stir bar for 7 days. After the experiment, the specimen was retrieved from the glass cell, rinsed with deoxygenated deionized water, dried with a cold air blower, placed in a vacuum desiccator for about 5 min, and sealed in a nitrogen purged, gas-filled, and sealed plastic bag. The bag was not opened until it was ready for analysis on the Raman microscope platform. The first scan result is line (a) in Fig. 5. Only two characteristic peaks for mackinawite [33] were detected, and the spectrum indicated no prominent sign of oxidation. After the first scan,

Table 1
Chemical composition (wt. %) of API 5L X65.

Fe%	Mn%	Ni%	Cr%	Cu%	Si%	Mo%	C%
97.3237	1.5052	0.2909	0.2519	0.1731	0.1668	0.0921	0.0454
V%	Nb%	Al%	Ti%	As%	N%	S%	Others%
0.0420	0.0338	0.0282	0.0120	0.0075	0.0067	<0.001	0.0136

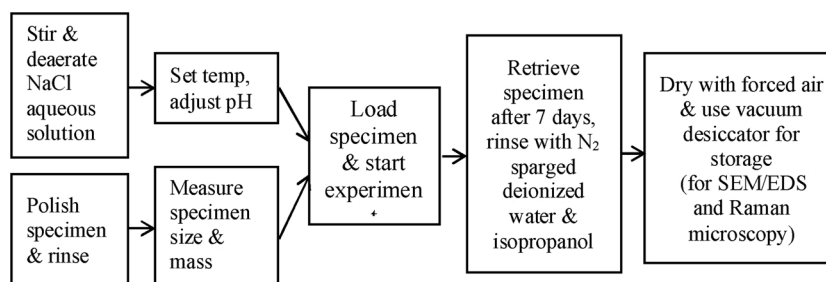


Fig. 3. Flow chart of experimental procedure.

Table 2

Test matrix of the effect of various oxygen ingress concentrations.

Temperature	30 °C		
pH	5.00 ± 0.01		
Material	API 5L X65		
P_{total}	1 bar		
P_{CO_2}	0.97 bar		
$P_{\text{H}_2\text{S}}$	0.04 mbar		
$[\text{O}_2]_{\text{aq}}$	Between 40 and 20 ppb _(w)	≈ 20 ppb _(w)	< 3 ppb _(w)
Glass Cell Setup	Stir bar	Impeller	Impeller
	Type (a)	Type (b)	Type (b)

Table 3

Possible explanations for the presence of oxides.

Hypothesis	Testing Methodology	Observation/Comments
#1. The specimen was oxidized before loading in the glass cell.	Collect Raman spectra of the freshly polished and rinsed specimens.	No peaks observed, implying no attachment of any oxides to the steel surface. This hypothesis was refuted.
#2. The corrosion product layer was oxidized after specimen retrieval from the glass cell and drying.	XRD, XPS, FIB-TEM and Raman to analyze the possible oxidation of the layer.	Mackinawite is oxidized easily in the air. The oxidizing speed depends on the thickness of the layer. Specimen preservation is needed in material analysis.
#3. Iron oxides form during the corrosion experiments due to oxygen ingress into the system.	Oxygen level monitored at the outlet scrubber of the system; Use of <i>in situ</i> Raman flow cell and flow loop.	Mackinawite corrosion product layer can be oxidized by $[\text{O}_2]_{\text{aq}}$ during the corrosion experiment.

another focus spot was selected, the second scan result after approximately 20 min exposure to air is line (b) in Fig. 5. Besides mackinawite, characteristic peaks for magnetite were also detected. The only explanation for this change is that mackinawite was oxidized in the air [28]. Then, a different spot was selected and a third Raman scan was conducted after approximately 60 min exposure to air, which is shown by line (c) in Fig. 5. Apart from mackinawite and magnetite, the third scan

also picked up hematite, which is a further oxidation product of mackinawite. This analysis shows that mackinawite is very sensitive to oxidation in air in plain daylight [29] and especially under the high intensity laser of a Raman microscope.

The extent of oxidation depended on the initial thickness of the FeS layer. In similar experiments, it has been noted that when the analyzed mackinawite layer was thinner than 100 nm, it had entirely turned yellow in color immediately after being retrieved from the glass cell. In the present case, the layer was thicker than 300 nm, so it is suspected that not all the layer was yet oxidized, as shown in the Raman spectrum collected as line (a) in Fig. 5. This observation confirmed that the second hypothesis in Table 3 is plausible: the magnetite identified by FIB-TEM-SAED in part I paper of this research project [18] could be an oxidation product of mackinawite after exposure to air, in post-processing analysis.

In order to address the third hypothesis listed in Table 3, O_2 content in the aqueous phase was monitored continuously with an oxygen meter for the entire duration of the test (as opposed to the beginning and end of the test only, as is commonly done), as shown in Fig. 6. The minimum O_2 content obtained for the best sealing case is listed in Fig. 7. It was achieved using the updated type (b) 2-liter glass cell with the sampling ports as shown in Fig. 2(b). The following observations could be made: (1) The initial two hours sparging with CO_2 or N_2 , before injection of H_2S , decreased the dissolved O_2 content from 8 ppm_(w) to 3 ppb_(w); (2) during the seven days of testing, dissolved O_2 content could reach as low as 3 ppb_(w) even though $\text{CO}_2/\text{H}_2\text{S}$ sparging was maintained; (3) loading/removing specimens (day 1, 3 and 7) through pulling specimens out from the sampling ports on the glass cell lid would lead to a temporary spike in dissolved O_2 up to 1 ppm_(w), slowly decreasing back to less than 3 ppb_(w) over a period of 20 min.

Table 4 shows some of the typical oxygen concentration in a glass cell reactor when a continuous gas flow of CO_2/N_2 with H_2S is sparged at ambient pressure at 30 °C. As shown in Fig. 7, the minimum oxygen content achievable in the type b glass cell setup was $[\text{O}_2]_{\text{aq}} = 3 \text{ ppb}_{(w)}$. Using the type (a) glass cell setup, the minimum level was $[\text{O}_2]_{\text{aq}} = 20 \text{ ppb}_{(w)}$ of dissolved oxygen, especially in long term experiments (e.g., 7 days). $[\text{O}_2]_{\text{aq}} = 8000 \text{ ppb}_{(w)}$ is the dissolved oxygen level in the atmosphere with 20 % of O_2 in the air. Considering the baseline conditions, the corresponding partial pressure of O_2 and H_2S are as follows: $p_{\text{O}_2} =$

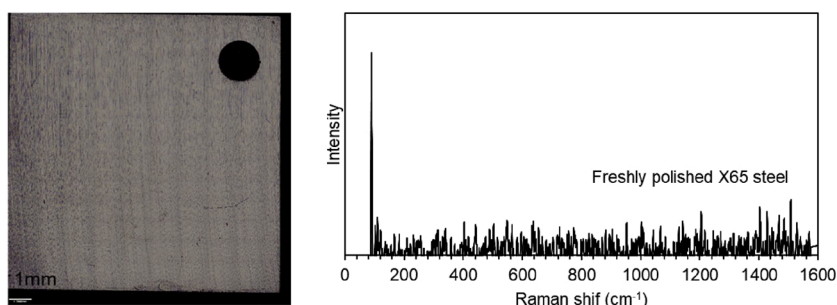


Fig. 4. No oxidation observed on freshly polished X65 specimen.

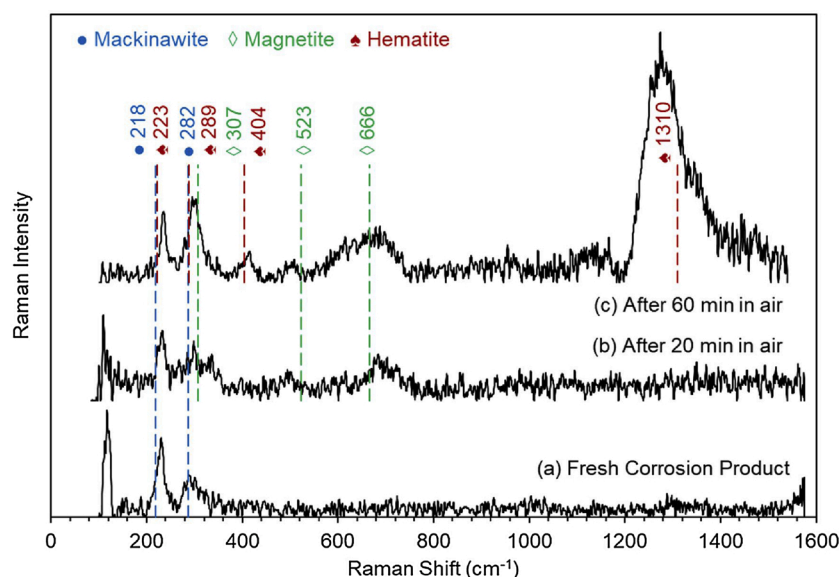


Fig. 5. Oxidation of mackinawite with time measured with a Raman microscope (laser excitation line 532 nm, power 25 W, the specimens were corroded at 30 °C, pH 5.01 ± 0.01, 0.97 bar CO₂, 0.04 mbar H₂S, 300 rpm stir bar, 7 days, [O₂]_{aq} ≈ 20 ~ 40 ppb_w).

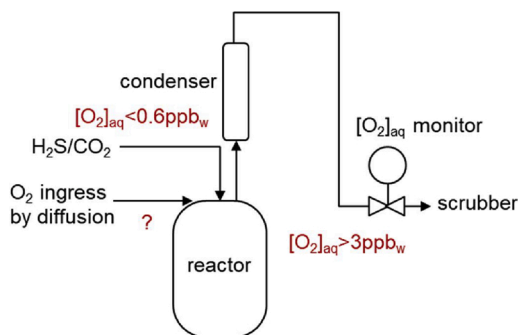


Fig. 6. Measuring dissolved oxygen concentration by placing oxygen meter at the end of the gas outlet of the experimental setup.

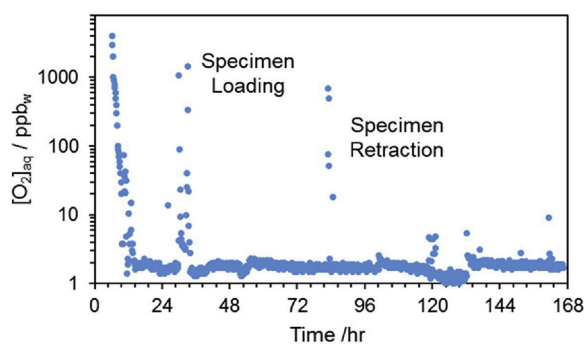


Fig. 7. Typical oxygen monitor results of a 7-day experiment in the type b setup as shown in Fig. 2(b).

7.92×10^{-5} bar (by oxygen meter) and $p_{\text{H}_2\text{S}} = 4 \times 10^{-5}$ bar (by gas detector tube). Although the dissolved H₂S concentration is 3.75×10^{-6} mol/L, which is 100 times more than the dissolved oxygen (9.38×10^{-8} mol/L), oxygen was continuously replenished in the cell due to diffusion and accumulated in the solution by oxidation reactions.

Only *in situ* observation of the oxidation of the FeS layer could directly prove that the presence of about 20 ~ 40 ppm_w of dissolved oxygen in solution was enough to alter the corrosion product layer

Table 4

Oxygen concentration in the experimental setup.

[O ₂] _{aq} /ppb _w *	[O ₂] _{aq} /(mol/L)	pO ₂ /bar	O ₂ gas content in the gas phase (ppm _v)
3	9.38×10^{-8}	7.92×10^{-5}	78
20	6.25×10^{-7}	5.28×10^{-4}	521
40	1.25×10^{-6}	1.06×10^{-3}	1042
8000	2.50×10^{-4}	2.11×10^{-1}	208508

* 1 ppb_w = 1 ng/g.

during an experiment. For that purpose, a specially designed cell was developed for *in situ* Raman spectroscopy analysis. Details of the *in situ* Raman cell design will be shown in another paper in preparation [34] and only the results are discussed here. Fig. 8 shows the experimentally acquired Raman spectrum of the corrosion product obtained *in situ* [spectrum (a)], the standard curve of oxidized mackinawite (FeS) [spectrum (b)], and the standard curve of magnetite (Fe₃O₄) [spectrum (c)]. The results confirmed that, under baseline condition with 20 ~ 40 ppb_w of dissolved oxygen, the corrosion product layer was made of mackinawite that was partially oxidized into magnetite. A peak corresponding to the carbonate group was also identified and likely corresponds to the presence of siderite (FeCO₃). This finding confirmed that the oxidation of mackinawite corrosion product layer into iron oxide, due to the presence of about 20 ppb_w of dissolved oxygen, can occur in sour corrosion experiments.

Consequently, the presence of oxides in the corrosion product layer composition can be explained by *in situ* as well as *ex situ* (post processing) oxidation of the mackinawite corrosion product layer.

While these preliminary results provided insight on the possible source of O₂ contamination, a more thorough and systematic study, performed in well-controlled environments, was warranted to differentiate the effects of trace amounts of O₂ present during the experiments, from the inevitable exposure to air in specimens post-processing.

4. Effect of various oxygen concentrations

The preliminary results, presented above, seem to indicate that even

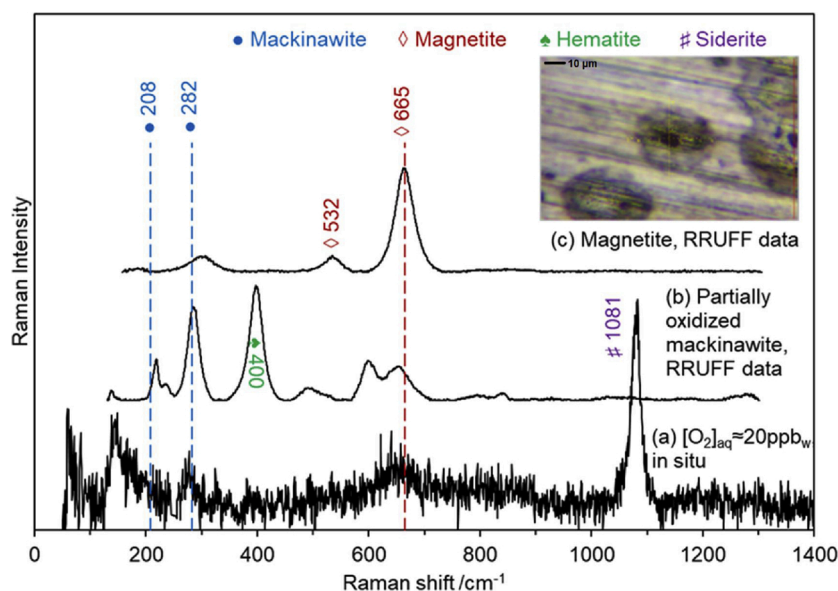


Fig. 8. *In situ* Raman spectroscopy analysis: direct proof of oxidation of mackinawite into magnetite in the aqueous solution on a corroding surface (Baseline condition with $[O_2]_{aq} = 3\sim 20$ ppb_(w), after 4 days).

traces of O_2 present during a test can influence both general and localized corrosion in marginally sour environments. To clarify this scenario, a series of experiments (Table 2) were designed and conducted in the improved setup (Fig. 2b), enabling better control of O_2 concentration in the aqueous phase. The results present the core of the discussion about this work.

Linear polarization resistant (LPR) and weight loss corrosion rates obtained from these three experiments are compared in Fig. 9. The general corrosion rate decreased as the oxygen concentration decreased. The basic mechanism of H_2S corrosion, without oxygen, dictates that H_2S should adsorb on the steel surface to form a chemisorbed FeS layer – $S_{ads}(Fe)$ [35]. More mackinawite could precipitate but only if the surface saturation value, $S(FeS)$, exceeds unity [36]. In the presence of less than 3 ppb_(w) dissolved O_2 , it is thought that the low corrosion rate (0.1 mm/y) was due to the protectiveness of the FeS chemisorbed layer since the FeS surface saturation never exceeded unity. However, for the experiment where around ca. 20 ppb_(w) of oxygen was maintained, the general corrosion rate was higher than the <3 ppb_(w) case (0.3 mm/y). The corrosion rate reached 0.9 mm/y when the oxygen ingress level is 20~40 ppb_(w). This experimental observation suggested that the

chemisorbed FeS layer, assuming it is unaffected by the presence of dissolved oxygen, provides most of the protection against corrosion. For comparison, similar conditions but without H_2S would yield a corrosion rate of 2~3 mm/y.

With less than 3 ppb_(w) of dissolved O_2 , TEM analysis in Figs. 10 and 11 shows that there was no visible layer at the surface after the 7 day corrosion test. Fig. 11 shows the Pt (orange) and Pd (green) plated layers on top of the steel surface (red). Fig. 11 also shows that there was no oxygen (blue) or sulfur (purple) near the surface. The presence of sulfur was detected but at the wrong location – above the Pd plated layer, which is obviously a mischaracterization and should be disregarded. The most plausible explanation for the low corrosion rate obtained in $O_2 < 3$ ppb_(w) condition is the presence of an extremely thin chemisorbed FeS layer protecting the surface.

In the presence of dissolved O_2 from 20 ppb_(w) to 40 ppb_(w), this chemisorbed layer could have been damaged, leading to higher corrosion rates. In turn, the release of Fe^{2+} increased the FeS surface saturation leading to the precipitation of a much thicker (100~300 nm) layer of FeS that could then be partially oxidized, as shown in Fig. 12. The corrosion mechanism and layer formation process in the presence of

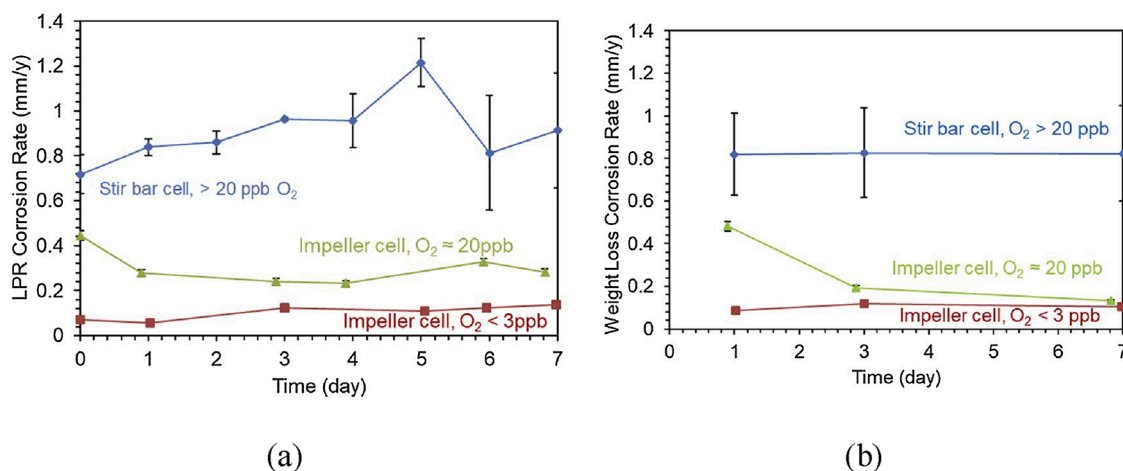


Fig. 9. Linear polarization resistance (a) and weight loss (b) corrosion rate (the specimens were corroded at 30 °C, pH = 5.01 ± 0.01, pCO₂ = 0.97 bar, pH₂S = 0.04 mbar, 300 rpm stir bar, 7 days).

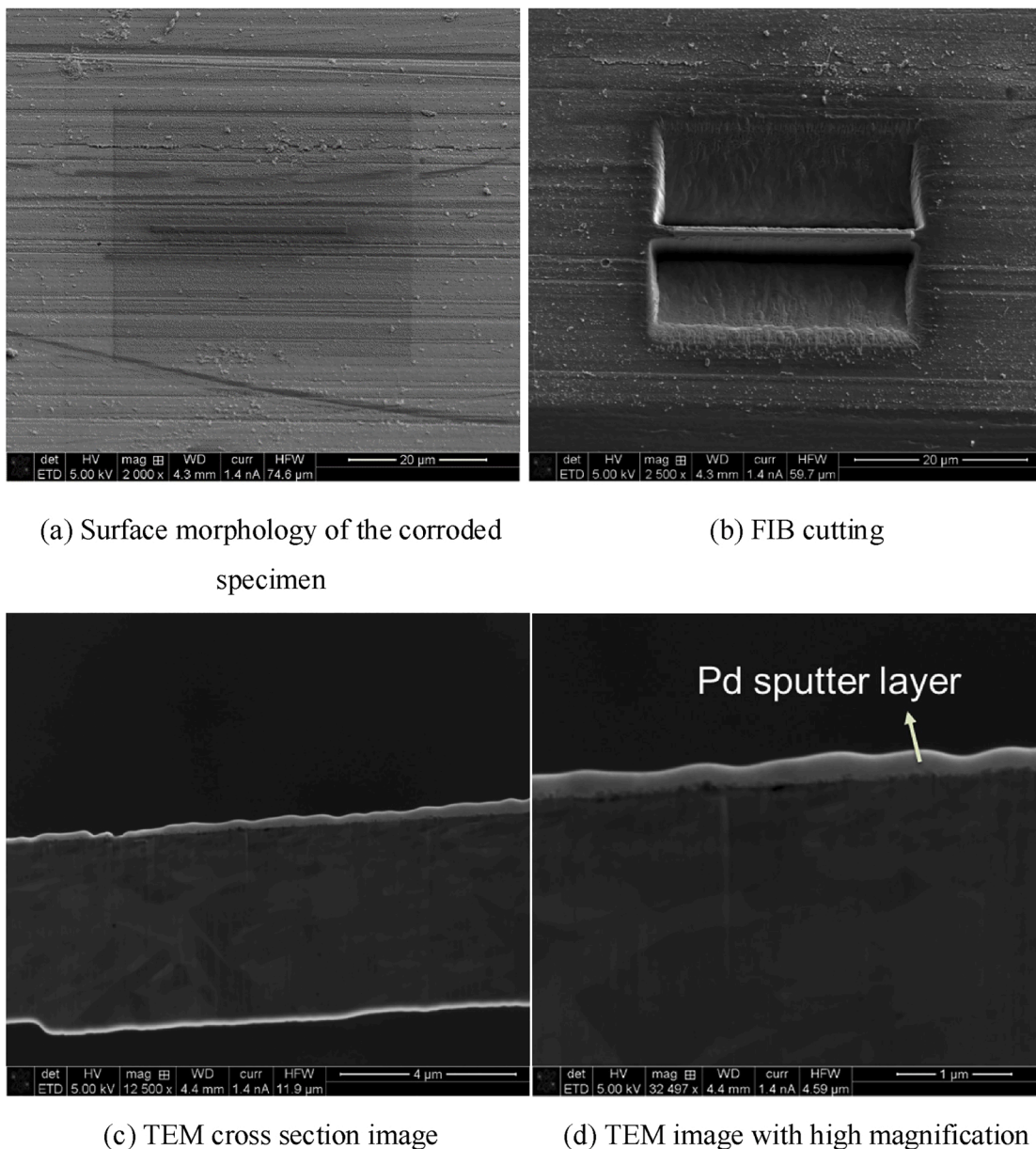


Fig. 10. FIB-TEM analysis of the corroded specimen with dissolved oxygen concentration less than 3 ppb_(w) (the specimens were corroded at 30 °C, pH 5, 0.97 bar CO₂, 0.04 mbar H₂S, 300 rpm stir bar, 7 days, [O₂]_(aq) < 3 ppb_(w)).

oxygen seem significantly more complex. The initial chemisorbed FeS layer may have been damaged by reaction with O₂, leading to exposure of the underlying metal and severe pitting corrosion. Once the chemisorbed FeS layer was damaged, the rate of metal loss was driven by the presence of corrosive CO₂. As a consequence, the increased corrosion rate led to an increase in pH and in FeS saturation level, then eventually to further precipitation of mackinawite that was unprotective.

In the conditions where [O₂]_{aq} < 3 ppb_(w), it is important to mention that no visible corrosion layer could be detected (Fig. 10). Efforts were made to confirm that a thin chemisorbed FeS layer could form on the steel surface. These efforts centered around the use of Pourbaix diagrams since experimental detection of chemisorbed layer using standard microscopy tools is difficult even with highly specialized equipment. The Pourbaix diagram (E-pH), shown in Fig. 13, was drawn considering both chemisorption and precipitation reactions based on literature data [35]. A direct observation based on this Pourbaix diagram shows that the thermodynamically most stable phase presents at lower pH in the diagram is the chemisorption layer of H₂S on steel surface – S_{ads}(Fe). These

data come from P. Marcus's adsorption experiments [35]. The large light blue area represents the domain of stability of chemisorbed S_{ads}(Fe). The small rectangle overlain on the diagram represents the actual experimental conditions of the baseline test (steel specimen OCP of 400~440 mV vs. SHE and pH = 5.00~5.10). The location of this baseline condition is outside the stability domain of mackinawite (grey-colored zone in the diagram). However, the baseline conditions do fall within the domain of stability of chemisorbed S_{ads}(Fe). It is hypothesized that the presence of this chemisorbed S_{ads}(Fe) film is enough to decrease the corrosion rate to 0.1 mm/y with 0.00004 bar H₂S in 1 bar CO₂. The thermodynamic calculation results seem to agree with the experimental observations. The main reactions applicable to the system are displayed below [35]:

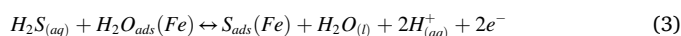


Fig. 14 shows the surface profilometry of the corroded specimens

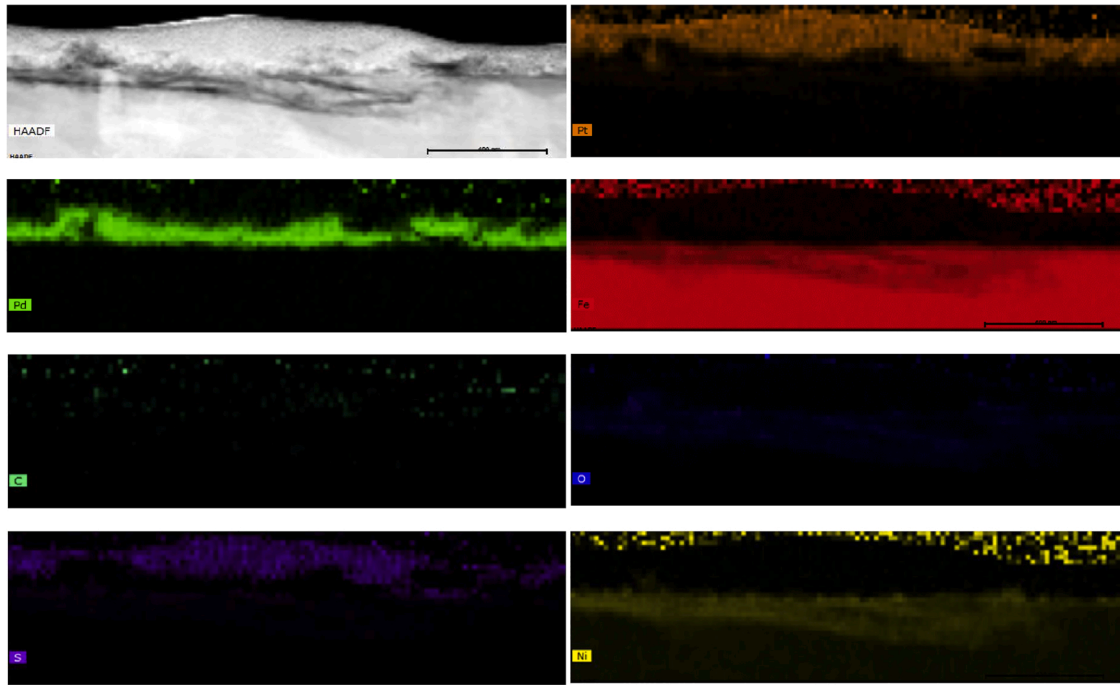


Fig. 11. TEM-EDS analysis of the corroded specimen with dissolved oxygen concentration less than 3 ppb(w) (the specimens were corroded at 30 °C, pH 5, 0.97 bar CO₂, 0.04 mbar H₂S, 300 rpm stir bar, 7 days, [O₂]_(aq) < 3 ppb_(w)).

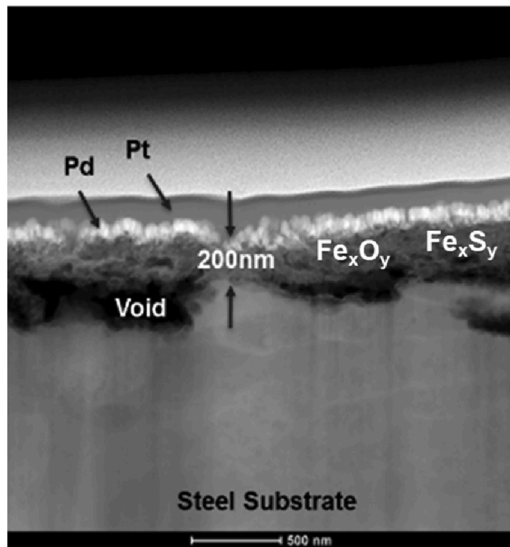


Fig. 12. TEM images of the cross section of the specimen for the baseline experiment cut out by FIB (30 °C, pCO₂ = 0.97 bar, pH₂S = 0.04 mbar, pH 5, X65, 1 wt.% NaCl, 300 rpm, 7 days, [O₂]_{aq} ≈ 20 ppb_(w)).

after the corrosion product layers were removed by Clarke solution [37]. Fig. 14(a) shows high pitting density and high pit penetration rates with [O₂]_(aq) > 20 ppb_(w). Fig. 14(b) ([O₂]_(aq) ≈ 20 ppb_(w)) shows lower pitting density (although the absolute density value is still high considering that the total area is as small as 1.6 cm²) and similar pit penetration rate compared with Fig. 14(a) ([O₂]_(aq) > 20 ppb_(w)). Fig. 14(c) ([O₂]_(aq) < 3 ppb_(w)) shows no pitting at all. Fig. 14(a) shows that the pits could be as deep as 120 μm after 7 days of exposure. It was developing after 14 days [38].

In summary, localized corrosion became a severe risk when oxygen concentration was higher than or equal to 20 ppb_(w) [O₂]_(aq) in marginally sour environments. In other words, only the “oxygen - free”

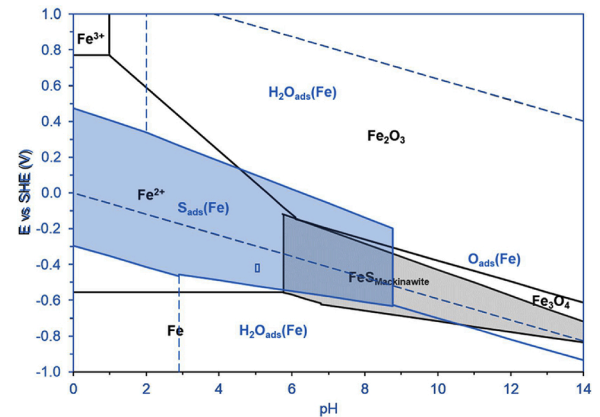


Fig. 13. Fe-S-H₂O Pourbaix diagram at 298.15 K considering chemisorbed layers, excluding the pyrite phase.

([O₂]_(aq) < 3 ppb_(w)) condition was able to eliminate the risk of pitting in marginally sour environments. It should be noted that the corrosion product layer became thinner as the oxygen concentration decreased. In the oxygen-free condition ([O₂]_(aq) < 3 ppb_(w)), it seems that there was no corrosion product layer formed at all. However, it has been documented that H₂S, unlike H₂CO₃, can be chemisorbed very easily onto the steel surface in aqueous solution [39]. The presence of this nanometer thick chemisorbed layer explains why the general corrosion rate was low, even if no layer could be visually detected on the steel surface (Figs. 10 and 11) when the oxygen content was less than 3 ppb_(w). It is somewhat counterintuitive, albeit well documented, that such a thin mackinawite layer (much less than 100 nm or only several layers of molecules) could decrease the general corrosion rate from 2 ~ 3 mm/y (in H₂S free environment) to about 0.1 mm/y. In addition, this layer seems to be very sensitive to even a trace amount of oxygen (more than 3 ppb_(w)). It can thereby be postulated that oxygen partially oxidized the metastable S_{ads}(Fe) layer, leading to inhomogeneities in the layer, and ultimately causing the occurrence of pitting. The exposed bare steel

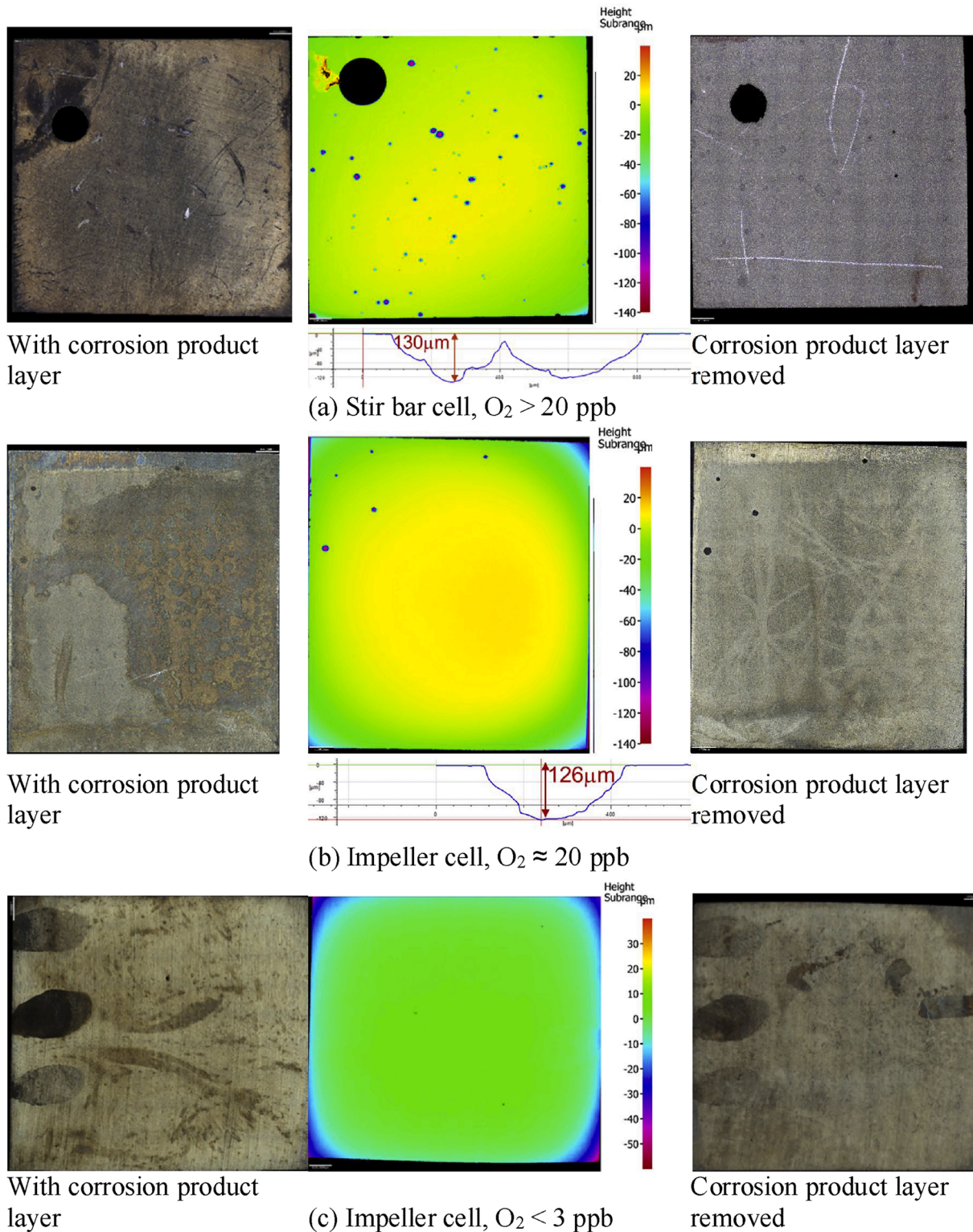


Fig. 14. Surface profilometry image after layer removal. (The specimens were corroded at 30 °C, pH 5.01 ± 0.01 , 0.97 bar CO_2 , 0.04 mbar H_2S , 300 rpm stir bar, 7 days).

locations were then exposed to the corrosive aqueous CO_2 environment at pH 5. A typical corrosion rate in this condition but without H_2S should be 2 ~ 3 mm/y, which is similar to the pitting corrosion measured on the steel specimens.

Fig. 15 shows the ferrous ion concentration measurements at different oxygen concentrations. The general trend is that the dissolved iron concentration increased with the increased general corrosion rate,

which was caused by the increase of oxygen concentration. It is important to mention that the spectrophotometry technique used to measure the iron ion concentration cannot discriminate between Fe^{2+} and Fe^{3+} and that the measurement result should be interpreted as the total dissolved iron ($[Fe^{3+}] + [Fe^{2+}]$) in the solution.

Increases or decreases in pH are expected in corrosion experiments due to the release of Fe^{2+} or the precipitation of metal carbonates or

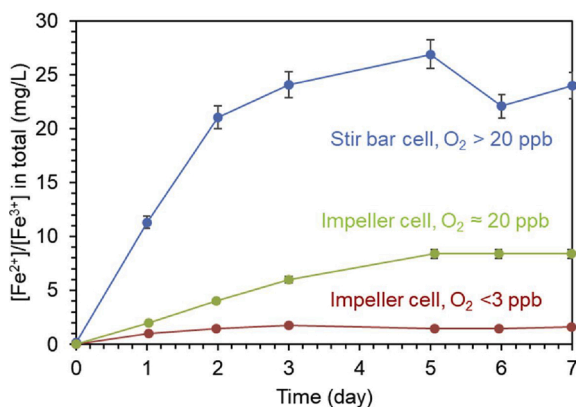


Fig. 15. The change of total amount of $[\text{Fe}^{2+}]/[\text{Fe}^{3+}]$ with time (the specimens were corroded at 30 °C, pH = 5.01 ± 0.01, pCO₂ = 0.97 bar, pH₂S = 0.04 mbar, 300 rpm stir bar, 7 days).

sulfides. As mentioned earlier, any change in pH was adjusted using the H-type exchange resin and this section discusses the tendency of the system to either increase or decrease the pH. Fig. 16 shows that pH had a tendency to decrease with time when $[\text{O}_2]_{(\text{aq})} < 3 \text{ ppb}_{(\text{w})}$, although this tendency is reversed when $[\text{O}_2]_{(\text{aq})} \approx 20 \text{ ppb}_{(\text{w})}$. As mentioned previously in the experimental setup section, the H-type ion exchange resin column could only decrease (not increase) the pH of the solution. Therefore, deoxygenated Na₂CO₃ solution was injected into the system through a syringe to bring the pH back to near 5.0 when necessary, so that corrosion rates at different O₂ concentration but the same other experimental conditions remained comparable.

Multiple reactions govern the pH in this system: 1) electrochemical reaction involving Fe and H₂S to produce Fe²⁺ and HS⁻ which tend to increase pH; 2) precipitation of FeS releases H⁺; 3) direct reduction of O₂ at the cathode consumes H⁺; 4) oxidation of H₂S by O₂ into sulfite [25], thiosulfate [26], or even sulfate [25] producing H⁺ ions in this process (through a process that might involve metal cations as a catalyst [40, 41]). Apparently, there is no simple linear relation between pH and O₂ content. It is important to mention that the extent of H₂S oxidation occurring in these sets of experiments is still a speculation at this stage. It is the subject of investigation presented in part III paper of this research project, which is about the catalytic oxidation of H₂S_(aq) by O_{2(aq)} contamination near steel surface at low temperatures in the aqueous solution [42].

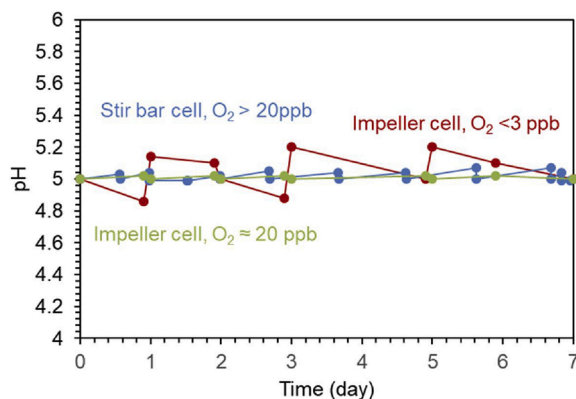


Fig. 16. pH changes with time (the specimens were corroded at 30 °C, 0.97 bar CO₂, 0.04 mbar H₂S, 300 rpm stir bar, 7 days).

5. Proposed mechanism of pit initiation in marginally sour environments

According to thermodynamic calculations in the Fe-S-H₂O system (see Fig. 13 [35]), a chemisorbed S_{ads}(Fe) film is very stable over a large area on the Pourbaix diagram, particularly in low pH conditions where precipitated iron sulfides are usually unstable. This S_{ads}(Fe) chemisorption film protects the steel surface from corrosive species such as H₂CO₃ or H⁺. However, this layer seems to be vulnerable to O₂ ingress and can be partially oxidized into iron oxides if enough dissolved O₂ is present, as shown by the *in situ* Raman spectrum in Fig. 8. Experimental observations showed that pit initiation occurred due to the presence of oxygen, which means that the phase change from iron sulfide to iron oxide is related to pit initiation. However, this does not automatically translate into part of steel surface being directly exposed to the corrosive environment. Afterall, Fe₃O₄ and Fe₂O₃ are very difficult to be dissolved in aqueous solution [43], just as FeS and NiS. This said, based on the fact that the single crystal volume of mackinawite, greigite, and magnetite are different, the total volume changes induced by the phase change from mackinawite to magnetite could be sufficient to expose part of the steel surface, leaving behind localized spots free of the protective layer that can then actively corrode. This pit initiation mechanism is schematically represented in Fig. 17.

The classic localized corrosion mechanism of the passive system is often compared with the mechanism of pitting in H₂S/CO₂ corrosion. Actually, the concept of passivation should be revisited to avoid confusion [44]. S_{ads}(Fe) layer in H₂S/CO₂ corrosion is similar to the passive layer in O₂ corrosion in terms of decreasing the uniform corrosion rate. However, the formation, structure, and properties of the two kinds of protective layers are quite different. The passive layer can be compromised by Cl⁻ [10]; while S_{ads}(Fe) layer can be compromised by O₂ contamination. Both S_{ads}(Fe) layer and its oxidation product Fe₃O₄ are difficult to be dissolved by H₂CO₃, but the cracks between the two phases can serve as the pit initiation sites. Fe-H₂O-H₂S/CO₂ localized corrosion has nothing to do with Cl⁻ [18]. Cl⁻ is detrimental to the passive system, which is the Fe-H₂O-O₂ system.

Pit propagation is caused by the Galvanic coupling effect and pit acidification, which has been published as part III of this investigation [38,42]. Galvanic coupling exists in this case because the corrosion product layer—mackinawite—is a metallic conductor. Pit acidification is caused by the catalytic oxidation of H₂S_(aq) by O_{2(aq)} into H⁺ and SO₄²⁻ [38,42].

Last but not the least, the proposed mechanism applies to marginally sour environments only. We (ICMT) defined the “marginally sour environment” as a layer-free condition where the partial pressure of H₂S is lower than the limit to meet the saturation unity of FeS(mackinawite) [1]. To calculate the saturation degree of FeS, speciation including [H⁺] are effective. For example, if one of the conditions such as pH changes, one can easily make the judgment by calculating the saturation of FeS. This is discussed in the Part I paper submitted to the same journal [18].

6. Conclusions

Trace amount of oxygen can cause pitting of mild steel in a marginally sour environment. This was verified by experiments at different oxygen concentrations (< 3 ppb_(w), 3 ~ 20 ppb_(w), 20 ~ 40 ppb_(w)) at baseline conditions of 30 °C, pH = 5.00 ± 0.01, pCO₂ = 0.97 bar, pH₂S = 0.04 mbar, 300 rpm stir bar, 7 days.

Specifically, for each experimental condition, the following observations can be made:

- No pitting occurred when the dissolved O₂ concentration was kept below 3 ppb_(w) during the entire duration of the test and no corrosion product could be identified with TEM. The general corrosion rate remained as low as 0.1 mm/y.

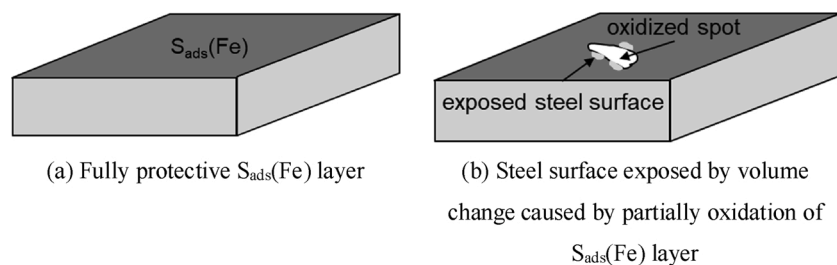


Fig. 17. Proposed mechanism of pit initiation in marginally sour environments.

- Pitting was found when the dissolved O_2 concentration was greater than or equal to 20 ppb_(w). A 200 nm thick corrosion product layer (mixture of iron sulfide and iron oxide) was identified with TEM. The general corrosion rate was about 0.8 mm/y.
- It is hypothesized that the dissolved O_2 partially oxidized the protective chemisorbed FeS layer, leaving small unprotected areas exposed to corrosive solution. This scenario can explain the initiation of localized corrosion.

This conclusion only applies to specific conditions in marginally sour environments (*i.e.*, low pH₂S and low pH). Previous research results [2] show that when the H₂S partial pressure was higher than 0.15 mbar or when the pH was higher than 6.00 ± 0.01 , no pitting occurred. This mode of localized corrosion could be mitigated either by eliminating dissolved oxygen or by increasing the pH of the aqueous environment.

Funding

This work was supported by the corrosion center joint industry project; Institute for Corrosion and Multiphase Technology, Ohio University, 342 West State Street, Athens, OH, 45701, USAGR0008847.01.

CRediT authorship contribution statement

Wei Zhang: Conceptualization, Methodology, Formal analysis, Investigation, Data curation, Writing - original draft, Visualization.
Bruce Brown: Methodology, Resources, Writing - review & editing, Project administration. **David Young:** Methodology, Writing - review & editing. **Marc Singer:** Conceptualization, Methodology, Writing - review & editing, Supervision, Funding acquisition.

Declaration of Competing Interest

The authors declare that they have no known competing financial interests or personal relationships that could have appeared to influence the work reported in this paper.

References

- [1] S. Navabzadeh Esmaeely, W. Zhang, B. Brown, M. Singer, S. Nešić, Localized corrosion of mild steel in marginally sour environments, *Corros. J.* 73 (9) (2017) 1098–1106.
- [2] W. Zhang, B. Brown, D. Young, S. Nestic, M. Singer, Factors influencing localized corrosion of mild steel in marginally sour environments, in: *NACE Corrosion Conf.*, Houston TX, 2018, p. 10984.
- [3] W. Yan, B. Brown, S. Nestic, Investigation of the threshold level of H₂S for pitting of mild steel in CO₂ aqueous solutions, in: *NACE Corrosion Conf.*, Phoenix, AZ, NACE, 2018, p. 11472.
- [4] B. Brown, D. Young, S. Nešić, Localized corrosion in an H₂S / CO₂ environment, in: *International Corrosion Congress/17*, NACE, Houston, TX, USA, 2009.
- [5] N. Yaakob, F. Farel, M. Singer, S. Nestic, D. Young, Localized top of the line corrosion in marginally sour environments, in: *NACE Corrosion Conf.*, NACE, Houston, TX, USA, 2016, p. 96026.
- [6] F. Pessu, R. Barker, A. Neville, Pitting and uniform corrosion of X65 carbon steel in sour corrosion environments: the influence of CO₂, H₂S, and Temperature, *Corros. J.* 73 (2017) 1168–1183.
- [7] F. Pessu, Y. Hua, R. Barker, A. Neville, A study of the pitting and uniform corrosion characteristics of X65 carbon steel in different H₂S-CO₂-containing environments, *Corros. J.* 74 (2018) 886–902.
- [8] B.F.M. Pots, R.C. John, Improvements on De Waard - Milliams corrosion prediction and applications to corrosion management, in: *NACE Corrosion Conf.*, Denver, CO, NACE, 2002, p. 02235.
- [9] S.N. Smith, Discussion of the history and relevance of the CO₂/H₂S ratio, in: *NACE Corrosion Conf.*, Houston, TX, 2011, p. 11065.
- [10] H. Strehblow, Mechanisms of pitting corrosion, in: P. Marcus (Ed.), *Corrosion Mechanisms in Theory and Practice*, Marcel Dekker, Inc., 2002.
- [11] J. Han, S. Nestic, Y. Yang, B.N. Brown, Spontaneous passivation observations during scale formation on mild steel in CO₂ brines, *Electrochim. Acta* 56 (2011) 5396–5404.
- [12] W. Li, Mechanical Effects of Flow on CO₂ Corrosion Inhibition of Carbon Steel Pipelines, Ph. D. Dissertation, Dept. Chem. & Biomol. Chem. Eng., Ohio Univ., Athens, OH, 2016.
- [13] E. Heitz, Chemo-mechanical effects of flow on corrosion, in: *NACE Corrosion Conf.*, Bally's Hotel, Las Vegas, Nevada, 1990, p. 1.
- [14] M. Parsi, K. Najmi, F. Najafifard, S. Hassani, B.S. McLauri, S.A. Shirazi, A comprehensive review of solid particle erosion modeling for oil and gas wells and pipelines applications, *J. Nat. Gas Sci. Eng.* 21 (2021) 850–873.
- [15] W. Sun, Kinetics of Iron Carbonate and Iron Sulfide Scale Formation in CO₂/H₂S Corrosion, Ph.D. Dissertation, Dept. Chem. & Biomol. Chem. Eng., Ohio Univ., Athens, OH, 2006, pp. 41–69.
- [16] Y. Sun, Localized CO₂ Corrosion in Horizontal Wet Gas Flow, Ph.D. Dissertation, Dept. Chem. & Biomol. Chem. Eng., Ohio Univ., Athens, OH, 2003, pp. 31–32.
- [17] E. van Hunnik, B.F.M. Pots, E.L.J.A. Hendriksen, The formation of protective FeCO₃ corrosion product layers in CO₂ corrosion, in: *NACE Corrosion Conf.*, Houston TX: NACE International, 1996, p. 6.
- [18] W. Zhang, B. Brown, D. Young, Gheorghe Bota, S. Nestic, M. Singer, "Pitting of mild steel in marginally sour environments – Part I: a parametric study based on protective layers formation", to be published in the same journal.
- [19] S. Wang, Effect of Oxygen on CO₂ Corrosion of Mild Steel, Master's Thesis, Ohio University, 2009.
- [20] N.R. Rosli, The Effect of Oxygen in Sweet Corrosion of Carbon Steel for Enhanced Oil Recovery Applications, Ph. D. Dissertation, Ohio University, 2015.
- [21] J. Han, B.N. Brown, D. Young, S. Nestic, Mesh-capped probe design for direct pH measurements at an actively corroding metal surface, *J. Appl. Electrochem.* 40 (2010) 683–690.
- [22] S. Gao, Thermodynamics and Kinetics of Hydrogen Sulfide Corrosion of Mild Steel at Elevated Temperatures, Ph. D. Dissertation, Ohio University, 2018.
- [23] S. Gao, B. Brown, D. Young, M. Singer, Formation of iron oxide and iron sulfide at high temperature and their effects on corrosion, *Corros. Sci.* 135 (2018) 167–176.
- [24] Y. Song, A. Palencsár, G. Svenningsen, J. Kvarekvål, T. Hemmingsen, Effect of O₂ and temperature on sour corrosion, in: *NACE Corrosion Conf.*, San Antonio, TX, NACE, 2014, p. 4299.
- [25] M.D. Deffo Ayagou, C. Mendibide, C. Duret-Thual, J. Kittel, K. Belkhadiri, T.T. Mai Tran, E. Sutter, B. Tribollet, N. Ferrando, Corrosion and hydrogen permeation in H₂S environments with O₂ contamination, 1: tests on pure iron at high H₂S concentration, *Corros. J.* 74 (11) (2018) 1192–1202.
- [26] J.L. Crolet, M. Pourbaix, A. Pourbaix, The role of trace amounts of oxygen on the corrosivity of H₂S media, in: *NACE Corrosion Conf.*, Houston, TX: NACE, 1991, p. 22.
- [27] D. Rickard, G.W. Luther III, Chemistry of iron sulfides, *Chem. Rev.* 107 (2007) 514–562.
- [28] G. Genchev, A. Erbe, Raman spectroscopy of mackinawite FeS in anodic iron sulfide corrosion products, *J. Electrochem. Soc.* 163 (6) (2016) C333–C338.
- [29] J. Holmes, Fate of incorporated metals during mackinawite oxidation in sea water, *Appl. Geochem.* 14 (1999) 277–281.
- [30] X. Zhong, B. Brown, W. Li, S. Nestic, M. Singer, How to maintain a stable solution chemistry when simulating CO₂ corrosion in a small volume laboratory system, in: *NACE Corrosion Conf.*, NACE, Houston, TX, USA, 2016, p. 7780.
- [31] Test Report, Method: Fe-10-M, Type Standard: N-NIST-1763a, by Laboratory Testing inc. May 14, 2014.
- [32] D.A. Jones, Thermodynamics and electrode potential. Principles and Prevention of Corrosion, 2nd ed., Prentice Hall, Upper Saddle River, NJ, 1996 ch.2, sec. 2.2: 59.
- [33] J.-A. Bourdoiseau, M. Jeannin, R. Sabot, C. Rémazeilles, Ph. Refait, Characterisation of mackinawite by Raman spectroscopy: Effects of crystallisation, drying and oxidation, *Corros. Sci.* 50 (2008) 3247–3255.

- [34] W. Zhang, D. Young, B. Brown, C. Shafer, F. Lu, E. Anyanwu, M. Singer, An in situ Raman study on the oxidation of mackinawite as corrosion product layer related to the pit initiation on mild steel in marginally sour environments, 2021.
- [35] P. Marcus, E. Protopopoff, Potential-pH diagrams for adsorbed species, application to sulfur adsorbed on iron in water at 25 °C and 300 °C, *J. Electrochem. Soc.* 137 (9) (1990) 2709–2712.
- [36] Y. Zheng, Electrochemical Mechanism and Model of H₂S Corrosion of Carbon Steel, Ph.D. Dissertation, Dept. Chem. & Biomol. Chem. Eng., Ohio Univ., Athens, OH, 2014, pp. 35–36.
- [37] ASTM G1-03, Standard Practice for Preparing, Cleaning, and Evaluating Corrosion Test Specimens, e1, ASTM International, West Conshohocken, PA, 2017, p. 2017, www.astm.org.
- [38] W. Zhang, Initiation and Propagation of Localized Corrosion of Mild Steel in Marginally Sour Environments, PhD Dissertation, Ohio University, 2020. Dec.
- [39] P. Marcus, E. Protopopoff, Potential-pH diagrams for adsorbed species, application to sulfur adsorbed on iron in water at 25 °C and 300 °C, *J. Electrochem. Soc.* 137 (9) (1990) 2709–2712.
- [40] S. Ma, A. Noble, D. Butcher, R.E. Trouwborst, G.W. Luther III, Removal of H₂S via an iron catalytic cycle and iron sulfide precipitation in the water column of dead end tributaries, *Estuar. Coast. Shelf Sci.* 70 (2006) 461–472.
- [41] E.S. Snavely, F.E. Blount, Rates of reaction of dissolved oxygen with scavengers in sweet and sour brines, in: NACE Corrosion Conf., Houston, Texas, 1969, p. 45.
- [42] W. Zhang, David Young, Bruce Brown, S. Nestic, M. Singer, Pitting of Mild Steel in Marginally Sour Environments – Part III: Pit Propagation Based on Acidification by Catalytic Oxidation of Dissolved Hydrogen Sulfide, 2021 paper draft to be submitted for publication.
- [43] U. Schwertmann, Solubility and dissolution of iron oxides, *Plant Soil* 130 (1991) 1–25.
- [44] H. Uhlig, Passivity in metals and alloys, *Corro. Sci.* 19 (1979) 777–791.